Chaos
An Interdisciplinary Journal of Nonlinear Science

RESEARCH ARTICLE | FEBRUARY 18 2025

# A recursive method to find the extreme and superstable curves in the parameter space of dissipative one-dimensional mappings

**Special Collection:** From Sand to Shrimps: In Honor of Professor Jason A. C. Gallas

Diogo Ricardo da Costa ; Luam Silva de Paiva ; Julia G. S. Rocha ; Joelson D. V. Hermes ; Matheus Hansen ; Ricardo Luiz Viana ; Iberê Luiz Caldas ; Rene O. Medrano-T

Check for updates

*Chaos* 35, 023146 (2025)
https://doi.org/10.1063/5.0239022

View Online
Export Citation

Articles You May Be Interested In

Dynamical properties of the composed Logistic–Gauss map

*Chaos* (January 2025)

A note on chaotic unimodal maps and applications

*Chaos* (August 2006)

Logistic map trajectory distributions: Renormalization-group, entropy, and criticality at the transition to chaos

*Chaos* (March 2021)

19 February 2025 18:38:27

AIP Publishing
Chaos
Special Topics Open for Submissions
Learn More

AIP Publishing

# A recursive method to find the extreme and superstable curves in the parameter space of dissipative one-dimensional mappings

Cite as: Chaos 35, 023146 (2025); doi: 10.1063/5.0239022
Submitted: 16 September 2024 · Accepted: 29 December 2024 ·
Published Online: 18 February 2025

View Online Export Citation CrossMark

Diogo Ricardo da Costa,[1,a)] Luam Silva de Paiva,[1] Julia G. S. Rocha,[1] Joelson D. V. Hermes,[2,3] Matheus Hansen,[4] Ricardo Luiz Viana,[5] Iberê Luiz Caldas,[3] and Rene O. Medrano-T[1,6]

## AFFILIATIONS

[1]Department of Physics, São Paulo State University—UNESP, 13506-900 Rio Claro, SP, Brazil
[2]Federal Institute of Education, Science and Technology of South of Minas Gerais—IFSULDEMINAS, 37576-000 Inconfidentes, MG, Brazil
[3]Physics Institute, University of São Paulo—USP, 05508-090 São Paulo, SP, Brazil
[4]Center for Mathematics and Applications (NOVA Math), NOVA School of Science and Technology, Universidade NOVA de Lisboa, Quinta da Torre, 2829-516 Caparica, Portugal
[5]Department of Physics, Federal University of Paraná—UFPR, 82590-300 Curitiba, PR, Brazil
[6]Department of Physics, Federal University of São Paulo—UNIFESP, 09913-030 Diadema, SP, Brazil

**Note:** This paper is part of the Focus Issue, From Sand to Shrimps: In Honor of Professor Jason A. C. Gallas.
[a)]**Author to whom correspondence should be addressed:** diogocost2@gmail.com

## ABSTRACT

This paper presents a recursive method for identifying extreme and superstable curves in the parameter space of dissipative one-dimensional maps. The method begins by constructing an Archimedean spiral with a constant arc length. Subsequently, it identifies extreme and superstable curves by calculating an observable $\psi$. The spiral is used to locate a region where $\psi$ changes sign. When this occurs, a bisection method is applied to determine the first point on the desired superstable or extreme curve. Once the initial direction is established, the recursive method identifies subsequent points using an additional bisection method, iterating the process until the stopping conditions are met. The logistic-Gauss map demonstrates each step of the method, as it exhibits a wide variety of periodicity structures in the parameter space, including cyclic extreme and superstable curves, which contribute to the formation of period-adding structures. Examples of extreme and superstable curves obtained by the recursive method are presented. It is important to note that the proposed method is generalizable and can be adapted to any one-dimensional map.

*Published under an exclusive license by AIP Publishing.* https://doi.org/10.1063/5.0239022

19 February 2025 18:38:27

**This paper presents a recursive method for identifying extreme and superstable curves in the parameter space of dissipative one-dimensional maps. The approach begins by constructing an Archimedean spiral with a constant arc length, which is then used to locate regions where an observable changes sign. This sign change indicates the presence of extreme or superstable curves, which are subsequently identified by using a bisection method. The method proceeds recursively, refining the search for these curves until predefined stopping conditions are met. The technique is applied to the logistic-Gauss map, which is known for its complex periodic structures, effectively demonstrating how the method uncovers cyclic extreme and superstable curves as well as period-adding structures. Moreover, the recursive approach is adaptable to any one-dimensional map, making it a robust and versatile tool for exploring parameter spaces in dissipative systems.**

## I. INTRODUCTION

In recent years, significant progress has been made in the study of nonlinear phenomena, introducing new concepts and approaches to the analysis of conservative and dissipative systems.[1–5] The literature includes several applications involving two-dimensional


Published under an exclusive license by AIP Publishing

maps,[6–8] such as the standard map,[9] the Fermi–Ulam model,[10,11] and others. If these systems preserve the area in phase space,[4,10] they are considered conservative; otherwise, they are dissipative, exhibiting forms of dissipation, such as viscosity or friction.

This paper focuses on the study of one-dimensional dissipative systems,[11–15] which can exhibit chaotic attractors and periodic fixed points.[16] To investigate the organization of periodic structures, we analyze the parameter space, constructed by varying two control parameters of the system. For each combination of control parameters, the corresponding Lyapunov exponent is calculated. In one-dimensional systems, a positive Lyapunov exponent indicates chaotic behavior, a negative value corresponds to periodic behavior, and a null exponent typically signifies bifurcations in the dynamics.

Lyapunov exponents[17–19] are a tool for analyzing the divergence or convergence of two initial conditions over time, enabling the identification of chaotic and periodic regions based on the color palette used in the parameter space. The study of such systems is a growing field of research, revealing a rich variety of complex periodic structures in parameter space diagrams,[8,20–22] bifurcations,[23–25] and foliations.[26,27] These investigations have direct applications in understanding and characterizing dynamical systems, including periodic structures embedded in chaotic domains and various mechanisms of self-organization and bifurcation.

When discussing parameter space, one cannot overlook Arnold's seminal article,[28] where he explored the organization of Arnold tongues. Following his work, there was a significant surge in interest in understanding periodicity windows, which are surrounded by chaotic attractors in parameter space. The organization of these periodic structures is governed by extreme and superstable curves.[23,29] These curves are crucial for studying periodicity windows, as their intersections provide valuable information about the system's dynamics. Specifically, they allow the determination of the period associated with the structure at the point of intersection. Additionally, cascades of periodicity windows are observed along extreme curves.[29] Superstable orbits, which exhibit very fast convergence as indicated by their Lyapunov exponent, are a key feature of these systems. The intersections of extreme curves not only reveal periodicity structures but also pinpoint the locations of superstable curves within the parameter space.

In this work, we present a highly accurate method for tracing extreme and superstable curves (both open and closed) with a comfortably large number of data points homogeneously distributed along the curves. The construction of our recursive method relies on Archimedean spirals,[30] which serve as the mechanism for locating the curves. These spirals are generated starting from an origin, with consecutive points spaced at a constant arc length.

We define an observable, denoted as $\psi$, that quantifies the distance from the desired curve. When $\psi$ changes sign—from positive to negative (or vice versa)—a bisection method is applied to pinpoint the first point on the curve. Once this initial point is identified, the optimal direction for the method to proceed is determined, and a new bisection method is used to iteratively find all subsequent points along the desired curve.

To validate the method, we apply it to the coupled logistic-like and Gauss mapping.[12] This mapping is particularly relevant as it exhibits various complex sets of periodicity (CSP). Of special interest is the phenomenon of the period-adding sequence, where the difference in periods between adjacent CSPs in an infinite sequence remains constant.[31–39] This phenomenon, observed in Ref. 12, highlights how extreme and superstable cyclic curves evolve as a function of a control parameter.

Our method can be seamlessly extended to multidimensional dynamical systems and to codimension-one bifurcation curves, including saddle-node, period-doubling, pitchfork, transcritical, and Andronov–Hopf bifurcations.

This paper is organized as follows: Sec. II introduces the test model, explains the differences between superstable and extreme orbits, and describes the process of obtaining the parameter space. Section III provides a detailed explanation of the proposed method. Finally, Section IV presents the concluding remarks.

## II. INITIAL CONSIDERATIONS

Before introducing the method proposed in this paper, it is essential to outline some key definitions. We begin by presenting an example of the mapping used to validate our recursive method. Next, we clarify the differences between superstable and extreme orbits. Finally, we describe the procedure for constructing the parameter space of a given model.

### A. Presenting our test model

To facilitate understanding of the step-by-step process involved in the recursive method, we apply the entire methodology to a specific example. The map considered in this paper is the one-dimensional logistic-Gauss mapping, introduced in Ref. 12. As previously mentioned, its parameter space exhibits a rich variety of complex sets of periodicity (CSP). As demonstrated in the final section of the paper, this mapping reveals extreme and superstable cyclic curves, which signal the emergence of CSP in period-adding sequences and mark the onset of the period-adding phenomenon.

One can write the Logistic-Gauss (LG) map as follows:

$$X_{n+1} = e^{-\delta\left[X_n\left(1-X_n^{\gamma}\right)\right]^2} + \beta \equiv F(X_n), \tag{1}$$

where $\delta > 0$, $\gamma > 0$, and $\beta \in (-1, 1)$ are control parameters of the system. Note that $F(X_n) > 0$, and this function is not unimodal, meaning that $F(X_n)$ can be greater than one. We refer $X_0$ to a given initial condition of the trajectory composed of the set of points $X_0$, $X_1 = F(X_0)$, $X_2 = F^{(2)}(X_0) = F(X_1)$, and so on.

The critical values of $X$ for the extremes (maximums and minimums) of $F(X)$ are determined by solving the equation $F'(X) = 0$. In contrast to what is discussed in Ref. 12, we focus on even values of $\gamma$, specifically $\gamma = 2$, which yield five solutions,

$$\begin{gathered} X_{(1)} = -1, \quad X_{(2)} = -(1+\gamma)^{-1/\gamma}, \quad X_{(3)} = 0, \\ X_{(4)} = (1+\gamma)^{-1/\gamma}, \quad \text{and} \quad X_{(5)} = 1. \end{gathered} \tag{2}$$

These five critical values of $X$, shown in Eq. (2), lead to the five local extremes $Y_{(j)} = F^{(1)}(X_{(j)})$, with $j = \{1, 2, 3, 4, 5\}$. For odd values of $j$ (1, 3, or 5), we are dealing with local maximums, while for even values of $j$ (2 or 4), we have local minimums.

19 February 2025 18:38:27


Published under an exclusive license by AIP Publishing

### B. Differences between superstable and extreme orbits

We refer to $k$-extreme orbits as trajectories that connect solutions of Eq. (2) after $k$ iterations, i.e.,

$$X_{(i)} = F^{(k)}(X_{(j)}), \tag{3}$$

with $i \neq j$. A superstable periodic orbit is one that connects $X_{(i)}$ to itself after $k$ iterations; in other words,

$$X_{(i)} = F^{(k)}(X_{(i)}). \tag{4}$$

In this paper, we refer to $(k)^{i\to j}$ as a period-$k$ extreme orbit that connects $X_{(i)}$ to $X_{(j)}$ after $k$ iterations, while $[k]^i$ denotes a period-$k$ superstable orbit that connects $X_{(i)}$ to itself after $k$ iterations.

Figure 1 illustrates the differences between superstable and extreme orbits by considering the return map $X_0$ vs $X_1$. For example, in Fig. 1(a), we show an extreme curve that connects the maximum $Y_{(3)}$ at $X_{(3)}$ to the minimum $Y_{(4)}$ at $X_{(4)}$ after two iterations of the mapping. This extreme trajectory is denoted as $(2)^{3\to4}$. To construct this return map, we used $(\delta, \beta) = (6.52514, -0.14099)$. Figure 1(b) shows the result of iterating the map after reaching $(X_{(4)}, Y_{(4)})$. As seen, the blue orbit is periodic, meaning that after two iterations, it returns to its initial position. In fact, this orbit is more than just periodic; it is superstable because there is an extreme in its closed trajectory, specifically a local minimum in this case. This blue superstable orbit is denoted as $[2]^4$; i.e., it connects $X_{(4)}$ to itself after two iterations.

Figure 1(c) shows the combination of control parameters $(\delta, \beta) = (16.22074, -0.09097)$. It illustrates the red extreme $(1)^{4\to3}$, which connects the local minimum $Y_{(4)}$ to the maximum $Y_{(3)}$ after one iteration. In Fig. 1(d), we continue iterating the map twice, resulting in the blue curve. This blue orbit is also an extreme curve

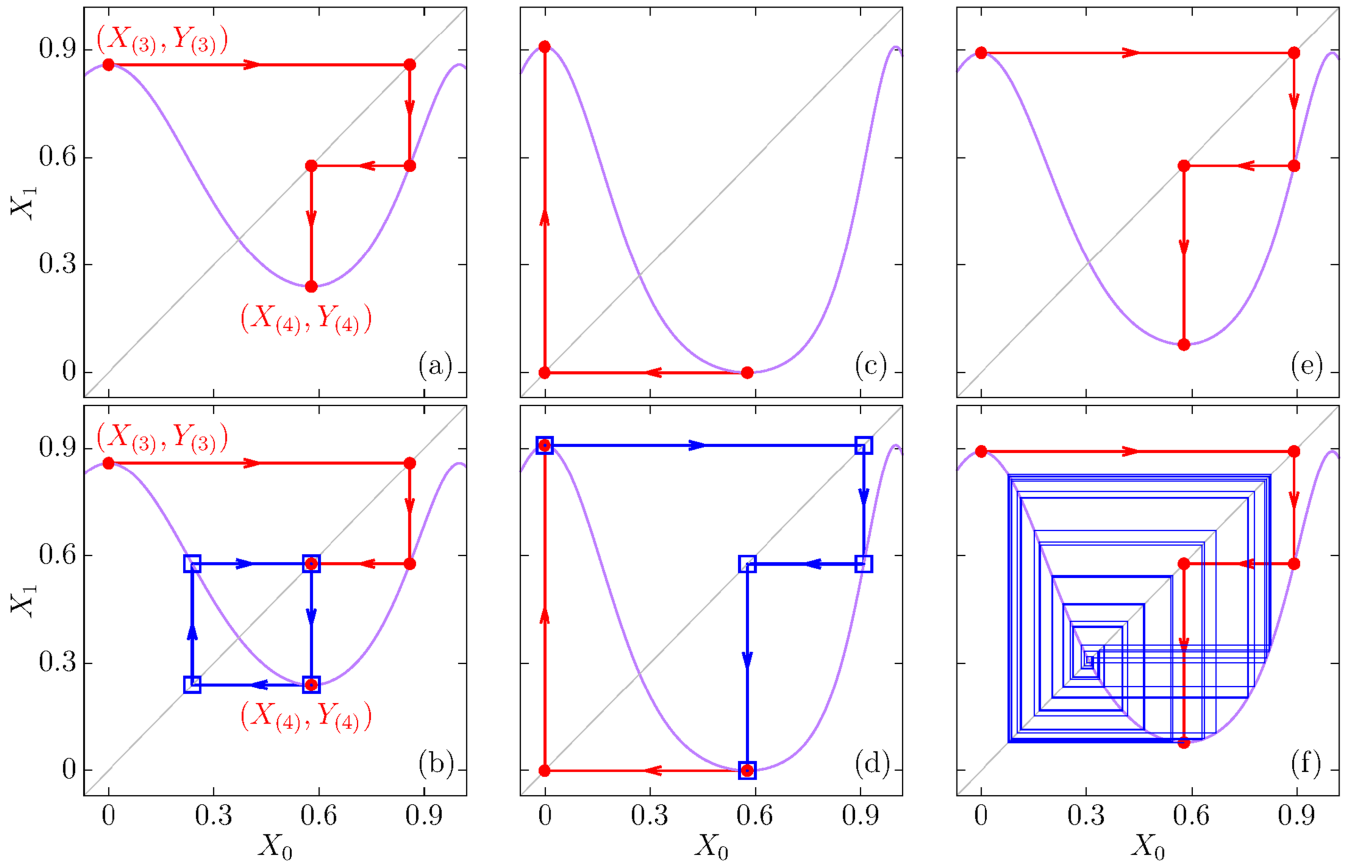



**FIG. 1.** In (a), we present the extreme $(2)^{3\to4}$, which connects a local maximum $Y_{(3)}$ at $X_{(3)}$ to a minimum $Y_{(4)}$ at $X_{(4)}$ after two iterations. This orbit, when iterated, as shown in (b), remains trapped in a period-2 superstable orbit (blue lines) named as $[2]^4$, i.e., connects a local minimum $Y_{(4)}$ at $X_{(4)}$ to itself after two iterations. Item (c) shows the extreme orbit $(1)^{4\to3}$ (red line), while (d) presents the extreme $(2)^{3\to4}$ (blue color). It is important to observe that the sum of the iterations of the extreme orbits gives the periodicity 3 of the superstable orbit (closed polygon). Item (e) shows the extreme orbit $(2)^{3\to4}$, and in item (f), we see that the extreme orbit is a transient to a chaotic attractor. To produce these plots, we considered the following combination of control parameters: (a) and (b) $\delta = 6.52514$ and $\beta = -0.14099$, (c) and (d) $\delta = 16.22074$ and $\beta = -0.09097$, and (e) and (f) $\delta = 11.3613$ and $\beta = -0.1081$. For all plots, we have $\gamma = 2$.

19 February 2025 18:38:27


Published under an exclusive license by AIP Publishing

that connects the local maximum to the minimum, denoted as $(2)^{3\to4}$. As seen, if we consider both the blue and red orbits, we obtain a closed orbit with period 3 (the sum of the interactions required to obtain both extremes). Here, we have two period-3 superstable curves coexisting, denoted as $[3]^3$ and $[3]^4$, along with the two extreme curves $(1)^{4\to3}$ and $(2)^{3\to4}$.

Figure 1(e) considers $(\delta, \beta) = (11.3613, -0.1081)$, where the extreme $(2)^{3\to4}$ appears in red. Figure 1(f) shows what happens when we continue iterating the map multiple times. Here, the orbit converges to a chaotic attractor (blue lines). This illustrates that an extreme orbit is not necessarily a periodic orbit; it can be a transient, as shown in this figure.

### C. How to get the parameter space of a model?

Figure 2 shows the parameter space $\delta$ vs $\beta$ for the LG mapping. To construct this parameter space, we consider a $1000 \times 1000$ grid of equally spaced points in the intervals $\beta \in [-0.8, 0]$ and $\delta \in [0, 25]$, while the last control parameter $\gamma = 2$ remains constant. For each combination of $(\delta, \beta)$, we set $X_0 = 0.2$ as the initial condition. Then, we calculate the Lyapunov exponent for the next $10^3$ iterations, after discarding a transient time of $10^3$ iterations. In such a situation, the Lyapunov exponent is

$$\lambda = \frac{1}{M}\sum_{j=1}^{M} \ln\left|F'(X)\right|, \tag{5}$$

where $M = 10^3$. The color palette, shown in Fig. 2, varies from red to yellow (negative Lyapunov exponent) for periodic regions and from green to blue (positive Lyapunov exponent) for chaotic regions. This plot shows periodic regions embedded within chaotic regions, along with superstable curves ($\lambda \ll 0$), highlighted in shades of red and embedded in yellow areas.

## III. A DETAILED EXPLANATION ABOUT OUR METHOD

The goal of this method is to find a selected extreme or superstable curve close to a given region of interest in the parameter space. For this purpose, we chose the Archimedean spiral, due to its linearly increasing size, which allows it to sweep the surrounding region homogeneously. The idea is to search for the intersection between the spiral and the curve. Once this point is identified, the next step is to find a sequence of points on the curve (in both directions) starting from this intersection. The condition we impose is that the distance between consecutive points on the curve must remain constant, independent of the scale used. For example, note the significant difference between the scales of the $\gamma$ and $\beta$ axes in Fig. 2. Below, we detail our method step by step.

### A. Archimedean spirals

Our main objective here is to derive a one-dimensional geometric object that can fill a surrounding space uniformly, independent of the scale used. Specifically, we aim to distribute points along this object in an equally spaced manner ($\Delta s = \text{const.}$) in order to locate extreme or superstable curves with very precise accuracy. For this purpose, we choose the Archimedean spiral, a special type of spiral that grows linearly with its size, described by the equation $r = A\theta$, where $r$ and $\theta$ are the polar coordinates in the plane, and $A > 0$. This results in the distance between consecutive revolutions being constant, $\Delta r = 2\pi A$.

From basic calculus, it is well known that the length of a curve in a planar space from point $a$ to point $b$ is given by $s = \int_a^b |\dot{z}|\, d\theta$, which means that a small variation of $s$ is

$$\Delta s \approx |\dot{z}|_a\, \Delta\theta, \tag{6}$$

where $\dot{z} = dz/d\theta$ with $z(\theta) = (r(\theta)\cos\theta, r(\theta)\sin\theta)$. Returning to the Archimedean spiral, let us consider a point $(r_m, \theta_m)$ along the spiral. Then, the next point is determined by $r_{m+1} = A\theta_{m+1}$ and,

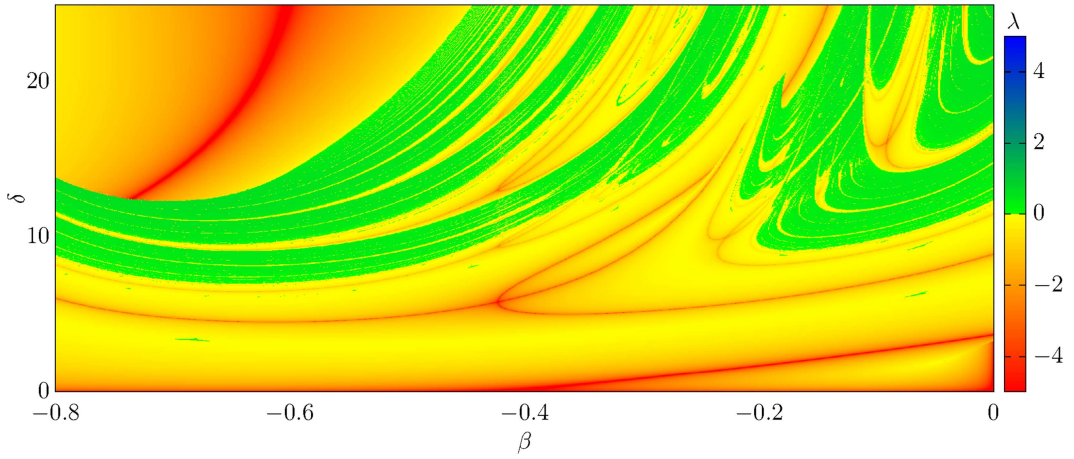



**FIG. 2.** Parameter space $\delta$ vs $\beta$ for $\gamma = 2$. For each combination of $\beta$ and $\delta$, we consider $X_0 = 0.2$ as the initial condition. The color palette represents the Lyapunov exponent $\lambda$. We will use this parameter space as our study object to explain how to find superstable and extreme curves. It is important to say that we flipped the axis for visual aspects, but the method was entirely built with $\delta$ in the horizontal axis and $\beta$ in the vertical axis.

19 February 2025 18:38:27


Published under an exclusive license by AIP Publishing

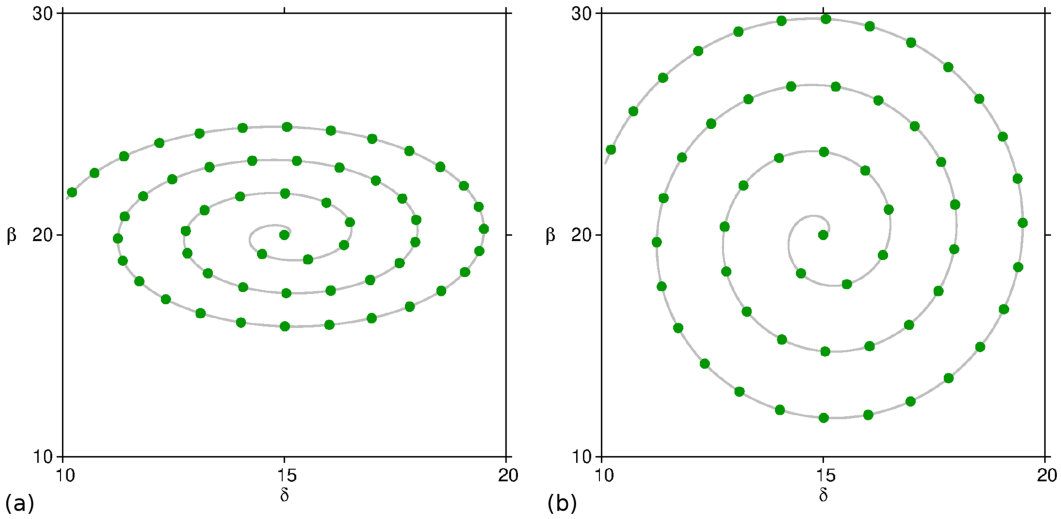



**FIG. 3.** (a) Archimedean spiral ($\Delta s = 1$ and $\Delta r = 1.5$) in the original axis scales of the graph, Eqs. (8) and (9). (b) Rescaled Archimedean spiral from Eqs. (10) and (11) with $\Delta s = 0.1$ and $\Delta r = 0.15$ rescaled according to the $\delta$ axis scale.

according to Eq. (6),

$$\theta_{m+1} \approx \theta_m + \frac{\Delta s}{A\sqrt{1+\theta_m^2}}, \tag{7}$$

where we deal with $|\dot{z}|_m = A\sqrt{1+\theta_m^2}$ and $\Delta\theta = \theta_{m+1} - \theta_m$. To guarantee the onset at the spiral focus, we set $\theta_1 = 0$.

Now, we consider that we have an available plot region on which we want to draw an Archimedean spiral, centered at $(\delta_c, \beta_c) = (15, 20)$, with points spaced by $\Delta s = 1$ and growing by $\Delta r = 1.5$ per revolution (Fig. 3). It has minimum and maximum values for both the vertical and horizontal axes. Our method will consider the value of $\delta \in [\delta_{\min}, \delta_{\max}]$ as the horizontal axis and $\beta \in [\beta_{\min}, \beta_{\max}]$ as our vertical axis. Defining

$$\Delta\delta = \delta_{\max} - \delta_{\min},$$
$$\Delta\beta = \beta_{\max} - \beta_{\min},$$

we call attention to the example shown in Fig. 3(a), where $\Delta\delta = 10$ and $\Delta\beta = 20$. This spiral was plotted by

$$\delta - \delta_c = r\cos\theta, \tag{8}$$

$$\beta - \beta_c = r\sin\theta, \tag{9}$$

with $r = \frac{1.5}{2\pi}\theta$ and $\theta$ incremented by $\Delta\theta = 2\pi/100$, starting from $\theta = 0$ for the gray curve, while for the green dots, it was determined from Eq. (7). Note that, since the scales of the axes are different ($\Delta\beta/\Delta\delta = 2$), the distances $\Delta s$ and $\Delta r$ do not appear constant, leading to some undesirable situations: (i) local concentration of points and (ii) regions of interest not covered by the spiral. To bypass these inconveniences, we rescale the variation in each axis to obtain the same geometric variation in both axes, i.e., $\delta - \delta_c \to (\delta - \delta_c)/\Delta\delta$ and $\beta - \beta_c \to (\beta - \beta_c)/\Delta\beta$. Applying these rescalings to Eqs. (8) and (9), the desired spiral, for a general case, has coordinates

$$\delta = \delta_c + A\theta\Delta\delta\cos\theta, \tag{10}$$

$$\beta = \beta c + A\theta\Delta\beta\sin\theta. \tag{11}$$

Electing, in Fig. 3(a), the geometric distances along the horizontal axis ($\delta$) as the optimum ones, $\Delta s = 1$ and $\Delta r = 1.5$, have to be rescaled to 0.1 and 0.15, respectively, to fix these distances as shown in Fig. 3(b).

### B. How to highlight extreme/superstable curves?

We define the observable $\psi$ as a measure of how far we are from our desired curve. This observable is defined as

$$\psi(\delta, \gamma, \beta, k, X_{(i)}, X_{(j)}) \equiv F^{(k)}(X_{(i)}) - X_{(j)}. \tag{12}$$

Here, $X_{(i)}$ and $X_{(j)}$ can assume one of the critical values shown in (2). For a period-$k$ superstable curve $[k]^i$, we need to have $X_{(i)} = X_{(j)}$, while for a $k$-extreme curve $(k)^{i\to j}$, we have $X_{(i)} \neq X_{(j)}$.

We will consider the same parameter region used in Fig. 2, i.e., $\delta \in [0, 25]$, $\beta \in [-0.8, 0]$, and $\gamma = 2$. We are going to search for a specific extreme or superstable curve. Let us start by giving one example: imagine you need to find the period-2 superstable curve that connects the local maximum $(X_{(3)}, Y_{(3)})$ to itself after two iterations (named $[2]^3$). Using Eq. (12), we need to consider $k = 2$ and $X_{(i)} = X_{(j)} = X_{(3)}$, so the observable $\psi$ for the superstable $[2]^3$ is

$$\psi(\delta, \beta) = F^{(2)}(X_{(3)}) - X_{(3)}. \tag{13}$$

For each combination of $\delta$ and $\beta$, we calculate the observable $\psi$. Figure 4(a) shows the result obtained. Here, negative values of $\psi$ are assigned a red-to-yellow color palette, while positive values are assigned a gradient from cyan to blue. The interface between the

19 February 2025 18:38:27


Published under an exclusive license by AIP Publishing

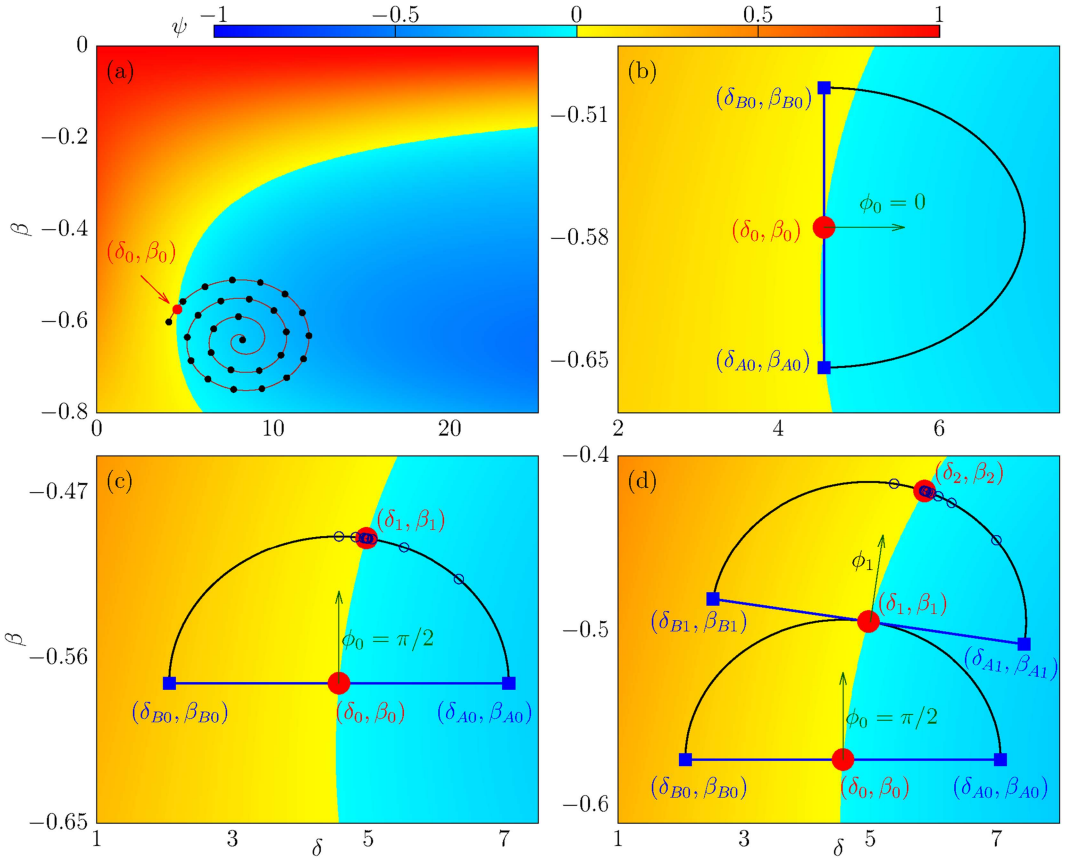



**FIG. 4.** This figure highlights a period-2 superstable curve that connects $(X_{(3)}, Y_{(3)})$ to itself after two iterations (named $[2]^3$). In (a), we considered $\delta \in [0, 25]$, $\beta \in [-0.8, 0]$, and $\gamma = 2$. The color palette represents the value of $\psi$ [see Eq. (13)]. First, we draw an Archimedean spiral with constant arc length $\Delta s = 8$, which is centered at the position $(\delta_c, \beta_c) = (8.25, -0.64)$. This spiral is used to find the solution $(\delta_0, \beta_0)$. Pictures (b), (c), and (d) are magnifications around $(\delta_0, \beta_0)$ illustrating the method to obtain the following points $(\delta_1, \beta_1)$ and $(\delta_2, \beta_2)$ (see detailed explanation in the text).

warm and cold colors identifies our superstable $[2]^3$, where $\psi \to 0$. Therefore, the fundamental idea is to find this interface.

### C. Searching for an initial point that belongs to the given curve

To find our superstable curve, we will consider an Archimedean spiral centered at the position $(\delta_c, \beta_c) = (8.25, -0.64)$. Figure 4(a) shows this spiral, which has a constant arc length $\Delta s = 8$. The center of the spiral starts in a region with $\psi < 0$ [according to Eq. (13)]. Each point on the spiral follows Eqs. (10) and (11) (with $A = 0.008$), where we constantly check if the value of $\psi$ enters a region where the sign changes. In our example, point number 27 reaches a region with positive $\psi$. After that, we apply a bisection method between points $[\delta_s(26), \beta_s(26)]$ (negative region) and $[\delta_s(27), \beta_s(27)]$ (positive region). The bisection method continues until $|\psi| \leq 10^{-10}$ (our tolerance value). When this occurs, we find the first point that belongs to the superstable $[2]^l$, here named as $(\delta_0, \beta_0)$ because it is our reference [see Fig. 4(a)].

### D. Finding the initial direction

Now, it is necessary to find an initial direction for the method. The angle $\phi_0$ is the direction we are moving toward the superstable curve [see Fig. 4(b)]. Observe that $\phi_0$ is also the direction of the semi-circle. In this example, we considered that $\phi_0$ can assume four values ($N_\phi = 4$): $\phi(1) = 0, \phi(2) = \pi/2, \phi(3) = \pi$, or $\phi(4) = 3\pi/2$. Just an observation: in our final code, we chose $N_\phi = 100$; i.e., we have 100 values for $\phi_0$ in the interval $\phi_0 \in [0, 2\pi)$. As this is just an example, let us continue with $N_\phi = 4$.

We start with $\phi_0 = \phi(1) = 0$ and calculate $\phi_a$ and $\phi_b$ as

$$\phi_a = \phi_0 - \pi/2 \quad \text{and} \quad \phi_b = \phi_0 + \pi/2. \tag{14}$$

Considering $R$ as the radius of the semi-circle, the symmetric points $P_{A0} = (\delta_{A0}, \beta_{A0})$ and $P_{B0} = (\delta_{B0}, \beta_{B0})$, shown in Fig. 4(b), are calculated as

$$\delta_{A0} = \delta_0 + R\Delta\delta \cos(\phi_a), \tag{15}$$

$$\beta_{A0} = \beta_0 + R\Delta\beta \sin(\phi_a), \tag{16}$$

19 February 2025 18:38:27


Published under an exclusive license by AIP Publishing

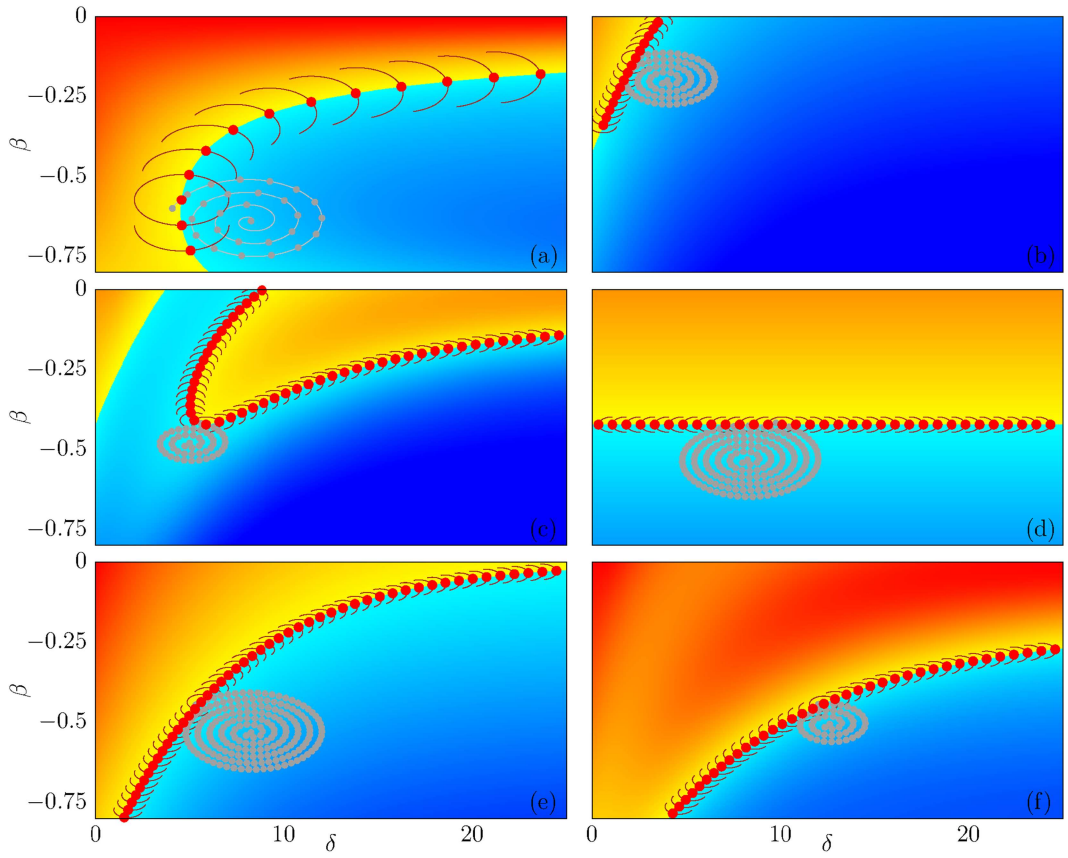



**FIG. 5.** In (a)–(c), we apply our method to find the superstable curves $[2]^3$, $[1]^4$, and $[2]^4$, while in (d)–(f), we use the method to find the extreme curves $(1)^{3\to4}$, $(1)^{4\to3}$, and $(2)^{3\to4}$. In (a), the spiral has $A = 0.008$ and $\Delta s = 8$, with a radius of the semi-circles equal to $R = 0.1$, while in (b)–(f), we considered $A = 0.004$, $\Delta s = 4$, and $R = 0.03$ for visual aspects.

$$\delta_{B0} = \delta_0 + R\Delta\delta\cos(\phi_b), \tag{17}$$

$$\beta_{B0} = \beta_0 + R\Delta\beta\sin(\phi_b). \tag{18}$$

The parameter $R$ is very important. It defines the distance between consecutive points that will compose the superstable curve of $[2]^3$. In Figs. 4 and 5, we fix $R = 0.1$, $\Delta\delta = 25$, and $\Delta\beta = 0.8$. By using Eq. (13), we can find the value of $\psi$ for the points $P_{A0}$ and $P_{B0}$, named as $\psi_{A0}$ and $\psi_{B0}$, as follows:

$$\psi_{A0} = \psi(\delta_{A0}, \beta_{A0}) \quad \text{and} \quad \psi_{B0} = \psi(\delta_{B0}, \beta_{B0}). \tag{19}$$

An important thing needs to happen here, $\psi_{A0}$ and $\psi_{B0}$ must be in regions with opposite signs, i.e.,

$$\psi_{A0} \times \psi_{B0} < 0. \tag{20}$$

In the example of Fig. 4(b), this multiplication is greater than zero because both $\psi_{A0}$ and $\psi_{B0}$ are greater than zero (both are in the same yellow region).

Now that we know that $\phi_0 = \phi(1) = 0$ does not work properly, we need to consider that $\phi_0 = \phi(2) = \pi/2$ (the second value for $\phi$). Figure 4(c) shows this simulation, where we need to recalculate $\psi_{A0}$ and $\psi_{B0}$ all over again by using Eqs. (14), (18), and (19). Here, the condition shown in Eq. (20) is satisfied, because $(\delta_{A0}, \beta_{A0})$ is inside a cold region, while $(\delta_{B0}, \beta_{B0})$ is in a warm region. When this happens, we consider that the angle $\phi_0 = \phi(2)$ is a good starting direction. If $\phi_0 = \phi(2)$ were not a good angle, it would be necessary to consider $\phi_0 = \phi(3)$ and then $\phi_0 = \phi(4)$, until finding a good direction.

### E. Finding the second point that belongs to the superstable curve

Now, we intend to find the point $(\delta_1, \beta_1)$ shown in Fig. 4(c). We can do this by finding $\phi_m$, which is the average between the angles $\phi_a$ and $\phi_b$, calculated as

$$\phi_m = \frac{\phi_a + \phi_b}{2}. \tag{21}$$

For this $\phi_m$, we calculate the corresponding point $(\delta_m, \beta_m)$ on the semi-circle. We obtain these coordinates by

$$\delta_m = \delta_0 + \Delta\delta R\cos(\phi_m) \quad \text{and} \quad \beta_m = \beta_0 + \Delta\delta R\sin(\phi_m). \tag{22}$$

19 February 2025 18:38:27


Published under an exclusive license by AIP Publishing

After that, we calculate the value of $\psi$ for this point as

$$\psi_m = \psi(\delta_m, \beta_m); \tag{23}$$

if $\psi_m \times \psi_{A0} < 0$, we consider that $\phi_a = \phi_m$; otherwise, $\phi_b = \phi_m$. We recalculate $\phi_m$ using Eq. (21), trying again to find the value of $\psi_m$ [through Eq. (23)]. This bisection method continues until $|\psi| < 10^{-10}$. When this happens, we consider that $(\delta_1, \beta_1) = (\delta_m, \beta_m)$. We show the result in Fig. 4(c), where one can see points converging to the red point $(\delta_1, \beta_1)$. The new angle $\phi$, called $\phi_1$, is

$$\phi_1 = \phi_m. \tag{24}$$

### F. Finding the next points

Now, we follow a similar procedure to find the next points that belong to the given superstable curve $[2]^3$. As we have a new direction $\phi_1$, we calculate $\phi_a$ and $\phi_b$ by substituting $\phi_0$ with $\phi_1$ in Eq. (14).

Points $(\delta_{A1}, \beta_{A1})$ and $(\delta_{B1}, \beta_{B1})$ in Fig. 4(d) are calculated through Eq. (18) by substituting $(\delta_{A0}, \beta_{A0})$ and $(\delta_{B0}, \beta_{B0})$ with $(\delta_{A1}, \beta_{A1})$ and $(\delta_{B1}, \beta_{B1})$, respectively.

After that, we find the value of $\phi_m$ by using Eq. (21), calculate $(\delta_m, \beta_m)$ by using Eq. (22), and the respective value of $\psi_m$ through Eq. (23). When the bisection method converges, we can say that we found $(\delta_2, \beta_2) = (\delta_m, \beta_m)$. Figure 4(d) shows the result, where we can see that there are points converging to the red point $(\delta_2, \beta_2)$.

### G. Stop condition and going to the opposite direction

Figure 5(a) shows the result obtained by applying our method. The stopping condition occurs when we reach one of the borders of the figure.

To construct the entire superstable/extreme curve, we also need to move in the opposite direction of $\phi_0$. Here, it is simply a matter of sending the semi-circles in the direction $\phi_0 \to \phi_0 + \pi$, and we expand the method in this other direction as well.

### H. Testing our method by finding other extreme and superstable curves

In Figs. 5(b) and 5(c), we apply our method to find the superstable curves $[1]^4$ and $[2]^4$, while in (d), (e), and (f), we find the

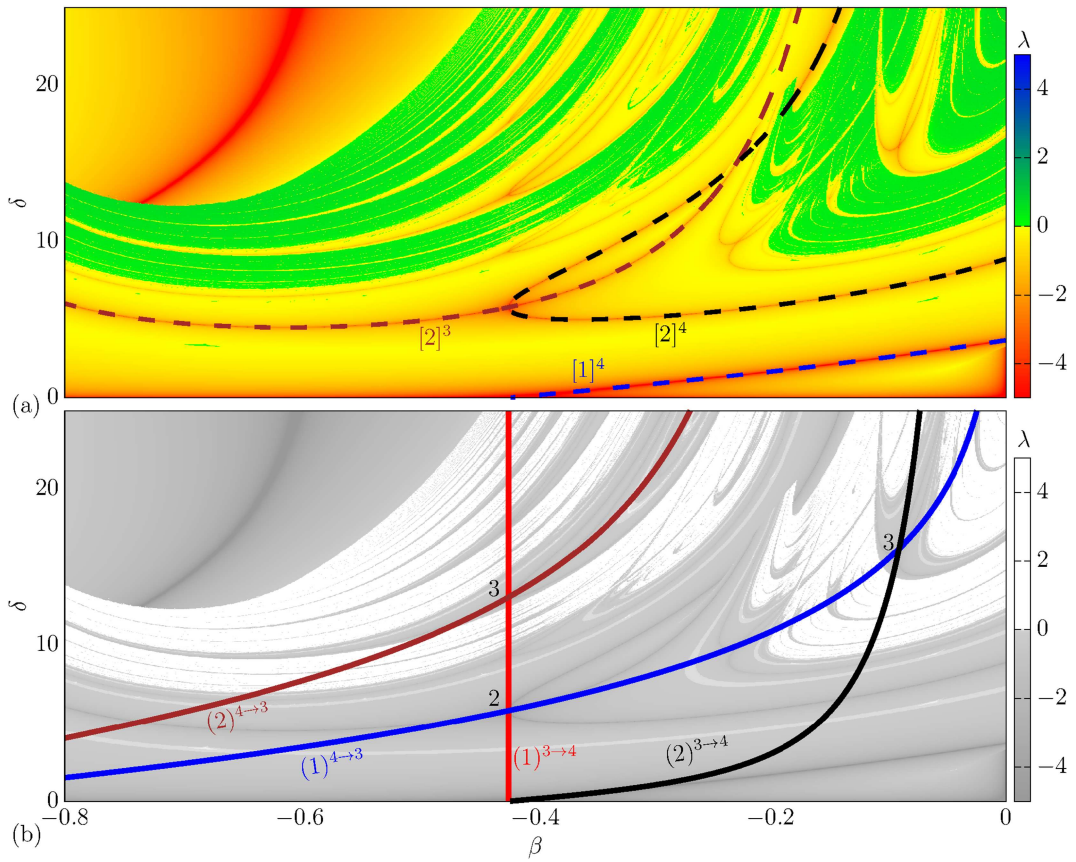



**FIG. 6.** In (a), we show the superstable curves $[1]^4$, $[2]^3$, and $[2]^4$ obtained by using our method. In (b), we show the extreme curves $(1)^{3\to4}$, $(1)^{4\to3}$, $(2)^{3\to4}$, and $(2)^{4\to3}$. Observe that the extreme curves $(1)^{3\to4}$ and $(1)^{4\to3}$ connect to each other in a period-2 CSP structure, which is the exact location where the extreme curves $[2]^3$ and $[2]^4$ connect in (a).

19 February 2025 18:38:27


Published under an exclusive license by AIP Publishing

extreme curves $(1)^{3\to4}$, $(1)^{3\to3}$, and $(2)^{3\to4}$. In Fig. 5(a), the spiral considers $A = 0.008$ and $\Delta s = 8$, with a radius of the semicircles equal to $R = 0.1$, while in Figs. 5(b), 5(c), 5(d), 5(e), and 5(f), we considered $A = 0.004$, $\Delta s = 4$, and $R = 0.03$ for visual aspects. As one can see, for all cases, we draw the extreme and superstable curves efficiently.

Observe that Fig. 5(b) shows the superstable curve $[1]^4$, but it also appears when we highlight the superstable curve $[2]^4$ in Fig. 5(c). This happens because the period-2 superstable is a multiple of the superstable curve with periodicity 1. A similar situation will occur when trying to highlight the superstable curve $[4]^4$, where we will also see the curves $[2]^4$ and $[1]^4$. Therefore, it is necessary to filter these curves. This issue (apparently) does not occur with the extreme curves.

In Figs. 6(a) and 6(b), we plotted the extreme and superstable curves obtained using our method. Figure 6(a) highlights the superstable curves $[1]^4$, $[2]^3$, and $[2]^4$, while Fig. 6(b) shows the extreme curves $(1)^{3\to4}$, $(1)^{4\to3}$, $(2)^{3\to4}$, and $(2)^{4\to3}$. Observe that the extreme curves $(1)^{3\to4}$ and $(1)^{4\to3}$ connect to each other in a period-2 CSP structure, which is the exact location where the superstable curves $[2]^3$ and $[2]^4$ are connected in Fig. 6(a). Additionally, the extreme curves $(2)^{3\to4}$ and $(1)^{4\to3}$ intersect in a period-3 CSP structure. The same occurs with the extreme curves $(2)^{4\to3}$ and $(1)^{3\to4}$, which also intersect in a period-3 CSP structure.

## I. Cyclic superstable/extreme curves

The stop condition for cyclic superstable and extreme curves occurs when both of the following conditions are met:

$$(\delta_j - \delta_0) \times (\delta_j - \delta_1) \le 0 \quad \text{and} \quad (\beta_j - \beta_0) \times (\beta_j - \beta_1) \le 0 \tag{25}$$

for $j \ge 2$. The method will continue until both conditions are met. We used this stop condition to find the superstable and extreme curves shown in Fig. 7.

These cyclic superstable and extreme curves are important because they illustrate the birth of period-adding cascades. Identifying these extreme curves is crucial for understanding the organization of periodic structures in the parameter space of dissipative systems.

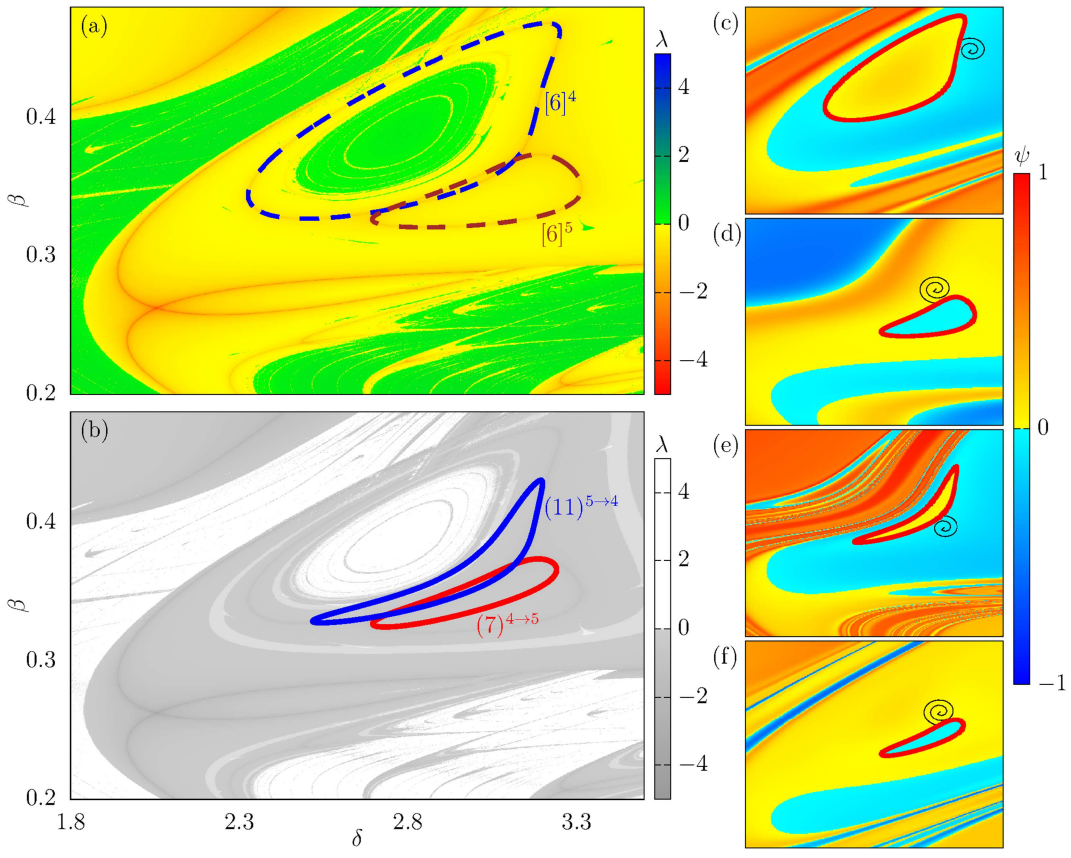



**FIG. 7.** Example of cyclic superstable and extreme curves. In (a), we show the superstable curves $[6]^4$ and $[6]^5$, while in (b), we present the extreme curves $(7)^{4\to5}$ and $(11)^{5\to4}$. In (c), (d), (e), and (f), we highlight the extreme and superstable curves using the observable $\psi$ for the curves $[6]^4$, $[6]^5$, $(7)^{4\to5}$, and $(11)^{5\to4}$, respectively.

19 February 2025 18:38:27


Published under an exclusive license by AIP Publishing

## IV. CONCLUSIONS

In this paper, we presented a recursive method to identify extreme and superstable curves in the parameter space of dissipative systems. We provided a detailed explanation of how our method worked. In summary, the method utilized an Archimedean spiral and defined an observable, denoted $\psi$. The spiral searched for regions where $\psi$ changes sign. Then, a bisection method was employed to find the first point on the extreme or superstable curve. Following this, the method determined a suitable direction and identified subsequent points. We applied our methodology to the logistic-Gauss mapping, which was particularly relevant due to its display of various complex periodic structures. Through this, we identified several extreme and superstable curves, demonstrating that the method was also applicable to cyclic extreme and superstable curves. Notably, we highlight that this recursive method can be adapted to any one-dimensional mapping and can also be extended to codimension-one bifurcations in multidimensional systems.

## ACKNOWLEDGMENTS

L.S.d.P. and J.G.S.R. acknowledge Coordenação de Aperfeiçoamento de Pessoal de Nível Superior-Brasil (CAPES). D.R.d.C., M.H., R.L.V., and I.L.C. acknowledge the São Paulo Research Foundation (FAPESP, Brazil) (Grant Nos. 2020/02415-7, 2019/09150-1, and 2018/03211-6) and the National Council for Scientific and Technological Development (CNPq) (Grant Nos. 162944/2020-0 and 301019/2019-3). M.H. was funded by national funds through the FCT—Fundação para a Ciência e a Tecnologia, I.P., under the scope of the projects UIDB/00297/2020 (https://doi.org/10.54499/UIDB/00297/2020) and UIDP/00297/2020 (https://doi.org/10.54499/UIDP/00297/2020) (Center for Mathematics and Applications). J.D.V.H. thanks the Federal Institute of Education, Science and Technology of South of Minas Gerais—IFSULDEMINAS. R.O.M.-T. acknowledges the partial support of the National Council for Scientific and Technological Development—CNPq, Project No. 408522/2023-2 and FAPESP—São Paulo Research Foundation through the grant 2024/06718-5.

## AUTHOR DECLARATIONS

### Conflict of Interest

The authors have no conflicts to disclose.

### Author Contributions

**Diogo Ricardo da Costa:** Conceptualization (lead); Data curation (equal); Formal analysis (equal); Investigation (lead); Methodology (lead); Software (equal); Supervision (lead); Validation (equal); Visualization (equal); Writing – original draft (equal); Writing – review & editing (equal). **Luam Silva de Paiva:** Conceptualization (equal); Investigation (equal); Methodology (equal); Software (equal); Validation (equal); Visualization (equal); Writing – original draft (equal); Writing – review & editing (equal). **Julia G. S. Rocha:** Conceptualization (equal); Investigation (equal); Methodology (equal); Software (equal); Validation (equal); Visualization (equal); Writing – original draft (equal); Writing – review & editing (equal). **Joelson D. V. Hermes:** Investigation (equal); Methodology (equal); Supervision (equal); Validation (equal); Visualization (equal); Writing – original draft (equal); Writing – review & editing (equal). **Matheus Hansen:** Conceptualization (equal); Investigation (equal); Methodology (equal); Validation (equal); Visualization (equal); Writing – original draft (equal); Writing – review & editing (equal). **Ricardo Luiz Viana:** Conceptualization (equal); Investigation (equal); Methodology (equal); Supervision (equal); Validation (equal); Visualization (equal); Writing – original draft (equal); Writing – review & editing (equal). **Iberê Luiz Caldas:** Conceptualization (equal); Investigation (equal); Methodology (equal); Validation (equal); Visualization (equal); Writing – original draft (equal); Writing – review & editing (equal). **Rene O. Medrano-T:** Conceptualization (equal); Data curation (equal); Investigation (equal); Methodology (equal); Software (equal); Supervision (equal); Validation (equal); Visualization (equal); Writing – original draft (equal); Writing – review & editing (equal).

## DATA AVAILABILITY

The data that support the findings of this study are available from the corresponding author upon reasonable request.

## REFERENCES

[1] J. Guckenheimer and P. Holmes, *Nonlinear Oscillations, Dynamical Systems, and Bifurcations of Vector Fields* (Springer Science & Business Media, 2013), Vol. 42.
[2] A. J. Lichtenberg and M. A. Lieberman, *Regular and Stochastic Motion* (Springer Science & Business Media, 2013), Vol. 38.
[3] B.-L. Hao, *Elementary Symbolic Dynamics and Chaos in Dissipative Systems* (World Scientific, 1989).
[4] A. J. Lichtenberg and M. A. Lieberman, *Regular and Chaotic Dynamics*, Applied Mathematical Sciences (Springer-Verlag, 1992).
[5] J. C. Willems, "Dissipative dynamical systems," Eur. J. Control **13**, 134–151 (2007).
[6] C. M. Kuwana, J. A. de Oliveira, and E. D. Leonel, "A family of dissipative two-dimensional mappings: Chaotic, regular and steady state dynamics investigation," Physica A **395**, 458–465 (2014).
[7] J. A. de Oliveira and E. D. Leonel, "Locating invariant tori for a family of two-dimensional Hamiltonian mappings," Physica A **390**, 3727–3731 (2011).
[8] J. A. De Oliveira, L. T. Montero, D. R. Da Costa, J. Méndez-Bermúdez, R. O. Medrano-T, and E. D. Leonel, "An investigation of the parameter space for a family of dissipative mappings," Chaos **29**, 053114 (2019).
[9] D. F. Oliveira, E. D. Leonel, and M. Robnik, "Boundary crisis and transient in a dissipative relativistic standard map," Phys. Lett. A **375**, 3365–3369 (2011).
[10] D. G. Ladeira and E. D. Leonel, "Dynamics of a charged particle in a dissipative Fermi–Ulam model," Commun. Nonlinear Sci. Numer. Simul. **20**, 546–558 (2015).
[11] D. R. da Costa, "A dissipative Fermi–Ulam model under two different kinds of dissipation," Commun. Nonlinear Sci. Numer. Simul. **22**, 1263–1274 (2015).
[12] D. R. da Costa, J. G. Rocha, L. S. de Paiva, and R. O. Medrano-T, "Logistic-like and Gauss coupled maps: The born of period-adding cascades," Chaos, Solitons Fractals **144**, 110688 (2021).
[13] D. da Costa, M. Hansen, R. Medrano-T, and E. Leonel, "Extreming curves and the parameter space of a generalized logistic mapping," J. Vib. Test. Syst. Dyn. **2**, 109 (2018).
[14] J. A. de Oliveira, H. M. de Mendonça, D. R. da Costa, and E. D. Leonel, "Effects of a parametric perturbation in the Hassell mapping," Chaos, Solitons Fractals **113**, 238–243 (2018).
[15] G. Ruiz and C. Tsallis, "Nonextensivity at the edge of chaos of a new universality class of one-dimensional unimodal dissipative maps," Eur. Phys. J. B **67**, 577–584 (2009).

19 February 2025 18:38:27


Published under an exclusive license by AIP Publishing

[16]E. D. Leonel, J. Kamphorst Leal da Silva, and S. Oliffson Kamphorst, "Transients in a time-dependent logistic map," Physica A **295**, 280–284 (2001).
[17]N. Fiedler-Ferrara and C. P. C. do Prado, *Caos: uma Introdução* (Editora Blucher, 1994).
[18]E. D. Leonel, *Invariância de Escala em Sistemas Dinâmicos Não Lineares* (Editora Blucher, 2019).
[19]E. Leonel, *Scaling Laws in Dynamical Systems*, Nonlinear Physical Science (Springer Nature, Singapore, 2021).
[20]C. E. P. Abreu, J. D. V. Hermes, D. R. da Costa, E. S. Medeiros, and R. O. Medrano-T, "Extreme fractal dimension at periodicity cascades in parameter spaces," Phys. Rev. E **110**, L032201 (2024).
[21]J. A. Gallas, "Structure of the parameter space of the Hénon map," Phys. Rev. Lett. **70**, 2714 (1993).
[22]E. Barreto, B. R. Hunt, C. Grebogi, and J. A. Yorke, "From high dimensional chaos to stable periodic orbits: The structure of parameter space," Phys. Rev. Lett. **78**, 4561 (1997).
[23]S. Fraser and R. Kapral, "Analysis of flow hysteresis by a one-dimensional map," Phys. Rev. A **25**, 3223 (1982).
[24]S. V. Gonchenko, "On a two parameter family of systems close to a system with a nontransversal Poincaré homoclinic curve: I," Selecta Math. Sovietica **10**, 69 (1991), translated from Methods of Qualitative Theory of Differential Equations; Ed. Gorky St. Univ., 1985, 55–72.
[25]S. V. Gonchenko, C. Simó, and A. Vieiro, "Richness of dynamics and global bifurcations in systems with a homoclinic figure-eight," Nonlinearity **26**, 621 (2013).
[26]J. P. Carcasses, C. Mira, M. Bosch, C. Simó, and J. C. Tatjer, ""Crossroad area–spring area" transition (I) parameter plane representation," Int. J. Bifurc. Chaos **1**, 183–196 (1991).
[27]C. Mira, ""Shrimp" fishing, or searching for foliation singularities of the parameter plane? Part I: Basic elements of the parameter plane foliation," **2016**(5), 1.
[28]V. I. Arnold, "Small denominators. I. Mapping the circle onto itself," Izv. Akad. Nauk SSSR Ser. Mat. **25**, 21–86 (1961), see https://www.mathnet.ru/php/archive.phtml?wshow=paper&jrnid=im&paperid=3366&option_lang=eng.
[29]D. R. Da Costa, M. Hansen, G. Guarise, R. O. Medrano-T, and E. D. Leonel, "The role of extreme orbits in the global organization of periodic regions in parameter space for one dimensional maps," Phys. Lett. A **380**, 1610–1614 (2016).
[30]A. C. de Sousa, E. Deckers, C. Claeys, and W. Desmet, "On the assembly of Archimedean spiral cavities for sound absorption applications: Design, optimization and experimental validation," Mech. Syst. Signal Process. **147**, 107102 (2021).
[31]K. Kaneko, "On the period-adding phenomena at the frequency locking in a one-dimensional mapping," Prog. Theor. Phys. **68**, 669–672 (1982).
[32]E. Yellin and A. Rabinovitch, "Properties and features of asymmetric partial devil's staircases deduced from piecewise linear maps," Phys. Rev. E **67**, 016202 (2003).
[33]C. Stegemann and P. C. Rech, "Organization of the dynamics in a parameter plane of a tumor growth mathematical model," Int. J. Bifurc. Chaos **24**, 1450023 (2014).
[34]S. L. T. de Souza, A. A. Lima, I. L. Caldas, R. O. Medrano-T, and Z. O. Guimarães-Filho, "Self-similarities of periodic structures for a discrete model of two-gene system," Phys. Lett. A **376**, 1290 (2012).
[35]E. S. Medeiros, R. O. Medrano-T, I. L. Caldas, and S. L. T. de Souza, "Torsion-adding and asymptotic winding number for periodic window sequences," Phys. Lett. A **377**, 628–631 (2013).
[36]V. English, U. Parlitz, and W. Lauterborn, "Comparison of winding-number sequences for symmetric and asymmetric oscillatory systems," Phys. Rev. E **92**, 022907 (2015).
[37]K. Klapcsik, R. Varga, and F. Hegedűs, "Bi-parametric topology of subharmonics of an asymmetric bubble oscillator at high dissipation rate," Nonlinear Dyn. **94**, 2373–2389 (2018).
[38]K. Klapcsik and F. Hegedűs, "Study of non-spherical bubble oscillations under acoustic irradiation in viscous liquid," Ultrason. Sonochem. **54**, 256–273 (2019).
[39]R. Varga, K. Klapcsik, and F. Hegedűs, "Route to shrimps: Dissipation driven formation of shrimp-shaped domains," Chaos, Solitons Fractals **130**, 109424 (2020).

19 February 2025 18:38:27


Published under an exclusive license by AIP Publishing